DOI:
10.1016/j.ica.2018.04.034

Document Version
Peer reviewed version

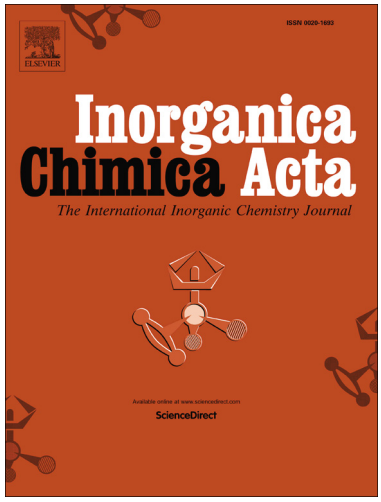

Research paper

Electrocatalytic proton reduction by thiolate-capped triiron clusters $[Fe_3(CO)_9(\mu_3\text{-}SR)(\mu\text{-}H)]$ (R = ^{i}Pr, ^{t}Bu)

Shishir Ghosh, Sucharita Basak-Modi, Michael G. Richmond, Ebbe Nordlander, Graeme Hogarth

PII: S0020-1693(18)30141-5
DOI: https://doi.org/10.1016/j.ica.2018.04.034
Reference: ICA 18225

To appear in: *Inorganica Chimica Acta*

Received Date: 25 January 2018
Revised Date: 10 April 2018
Accepted Date: 18 April 2018

Please cite this article as: S. Ghosh, S. Basak-Modi, M.G. Richmond, E. Nordlander, G. Hogarth, Electrocatalytic proton reduction by thiolate-capped triiron clusters $[Fe_3(CO)_9(\mu_3\text{-}SR)(\mu\text{-}H)]$ (R = ^{i}Pr, ^{t}Bu), *Inorganica Chimica Acta* (2018), doi: https://doi.org/10.1016/j.ica.2018.04.034

Electrocatalytic proton reduction by thiolate-capped triiron clusters $[Fe_3(CO)_9(\mu_3\text{-}SR)(\mu\text{-}H)]$ (R = ^{i}Pr, ^{t}Bu)

Shishir Ghosh [a,b], Sucharita Basak-Modi [a], Michael G. Richmond [c], Ebbe Nordlander [d], Graeme Hogarth [b,*]

[a] *Department of Chemistry, University College London, 20 Gordon Street, London WC1H 0AJ, U.K.*

[b] *Department of Chemistry, King's College London, Britannia House, 7 Trinity Street, London SE1 1DB, U.K.*

[c] *Department of Chemistry, University of North Texas, 1155 Union Circle, Box 305070, Denton, Texas 76203, U.S.A.*

[d] *Inorganic Chemistry Research Group, Chemical Physics, Center for Chemistry and Chemical Engineering, Lund University, Box 124,SE-221 00 Lund, Sweden*

ABSTRACT - The redox behaviour and electrocatalytic proton reduction ability of the thiolate-capped triiron clusters $[Fe_3(CO)_9(\mu_3\text{-}SR)(\mu\text{-}H)]$ (**1**, R = ^{i}Pr; **2**, R= ^{t}Bu) have been investigated. In CH_2Cl_2, both show a quasi-reversible reduction and an irreversible oxidation. The thiol substituent has a significant influence on their reduction potentials ($E_{1/2}$ = –1.24 V for **1** and $E_{1/2}$ = –1.40 V for **2** *vs.* Fc^+/Fc) but less impact on oxidation potentials ($E_{1/2}$ = 0.99 V for **1** and $E_{1/2}$ = 0.93 V for **2** *vs.* Fc^+/Fc). Reduction is quasi-reversible and DFT studies reveal that this is due to scission of an iron-iron bond. While the clusters are not protonated by CF_3CO_2H or $HBF_4{\cdot}Et_2O$, they can catalyse proton reduction of these acids at their corresponding reduction potentials following an ECEC mechanism.

Keywords: Triiron clusters; Thiolate; Electrocatalytic proton reduction; DFT studies

1. Introduction

Development of iron-based electrocatalysts for H_2 evolution is almost entirely centred on diiron complexes that are structural mimics of the active site(s) of [FeFe]-hydrogenase enzymes [1-5]. In contrast, the proton reduction ability of non-enzyme-related iron complexes has been relatively neglected even though the first report of electrocatalytic proton reduction by an iron complex was by [(TPP)Fe(Cl)] (TPP = tetraphenylporphyrin), which

catalyses proton reduction at reasonable catalytic rates [6]. Recently, other mononuclear iron catalysts have been developed by several groups, [7-15] some of which are able to catalyse proton reduction more efficiently than the majority of diiron biomimics [15].

Low-valent iron clusters have attracted attention as potential electrocatalysts due to the delocalized nature of bonding in the cluster core that can lead to low reduction potentials and stable reduced species [16-27]. Thus we and others have reported electrocatalytic proton reduction by the tetrairon nitrido-, carbido- and oxo-clusters $[NEt_4][Fe_4(CO)_{12}(\mu_4\text{-}N)]$ [16,17], $[NEt_4]_2[Fe_4(CO)_{12}(\mu_4\text{-}C)]$ [17] and $[Fe_4(CO)_{10}(\kappa^2\text{-dppn})(\mu_4\text{-}O)]$ [18], respectively, which show moderate catalytic activity in organic solvents with their sodium salts also being able to operate in water [17]. Recently, we also reported electrocatalytic reduction of protons by triiron clusters containing 2-aminopyridinate or 2-aminopyrimidinate ligand [28]. In addition, the sulfido-capped triiron cluster $[Fe_3(CO)_9(\mu_3\text{-}S)_2]$ [19,20] and the diphosphine derivatives, $[Fe_3(CO)_5(\kappa^2\text{-dppv})_2(\mu_3\text{-}S)_2]$ [21] (dppv = 1,2-bis(diphenylphosphino)ethylene) and $[Fe_3(CO)_7(\mu\text{-dppm})(\mu_3\text{-}S)_2]$ [22] (dppm = bis(diphenylphosphino)methane), have also been studied as proton reduction catalysts (Chart 1). The parent cluster $[Fe_3(CO)_9(\mu_3\text{-}S)_2]$ is not readily protonated even by strong acids but is catalytically active for hydrogen production at its second reduction potential in the presence of acetic acid [20], and at its first reduction potential in presence of $HBF_4{\cdot}Et_2O$ [19]. The diphosphine derivative $[Fe_3(CO)_5(\kappa^2\text{-dppv})_2(\mu_3\text{-}S)_2]$, with a more electron-rich cluster core, is protonated by strong acids such as $HBF_4{\cdot}Et_2O$ and displays catalysis initiated by protonation [21]. Recently, we have also investigated the selenide- and telluride-derivatives of $[Fe_3(CO)_9(\mu_3\text{-}S)_2]$ (Chart 1) and found that the nature of the chalcogenide exerts a significant influence on their redox response and electrochemical properties [23].

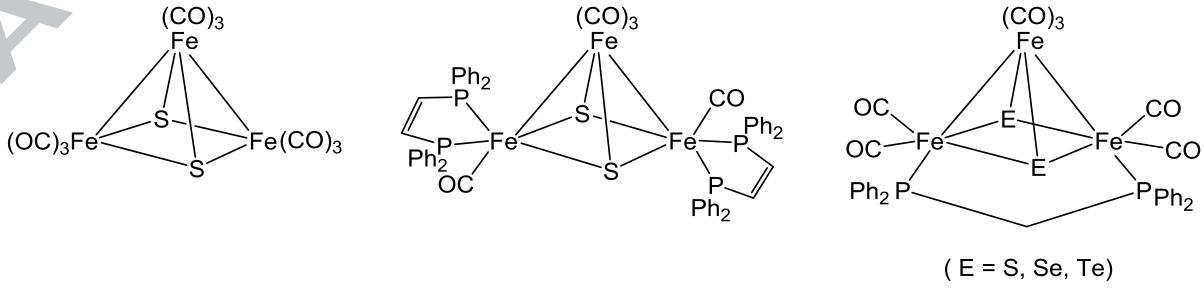

Chart 1. Chalcogenide-capped triiron clusters tested as proton reduction catalysts [19-23].

Low-valent thiolate-capped triiron clusters are thus potential candidates as electrocatalytic proton reduction catalysts. A number of such triiron clusters have been reported [29-33] and as part of a preliminary study we have tested two of these, namely $[Fe_3(CO)_9(\mu_3\text{-}S^iPr)(\mu\text{-}H)]$ (**1**) and $[Fe_3(CO)_9(\mu_3\text{-}S^tBu)(\mu\text{-}H)]$ (**2**), as electrocatalysts. Both clusters are capable of reducing protons in their monoanionic state and DFT calculations have been carried out in order to understand the nature of the key radical anion intermediate in the catalytic process.

2. Results and discussion

2.1. Synthesis and structure of $[Fe_3(CO)_9(\mu_3\text{-}SR)(\mu\text{-}H)]$ (R = ^{i}Pr, ^{t}Bu)

Clusters **1** and **2** were first synthesized by Beer and Haines in 1970 from the direct reaction between equimolar amounts of $[Fe_3(CO)_{12}]$ and RSH (R = ^{i}Pr, ^{t}Bu) at 80 °C (Scheme 1) [29]. Both were characterised by spectroscopic data [29], and later by X-ray crystallography [32,33].

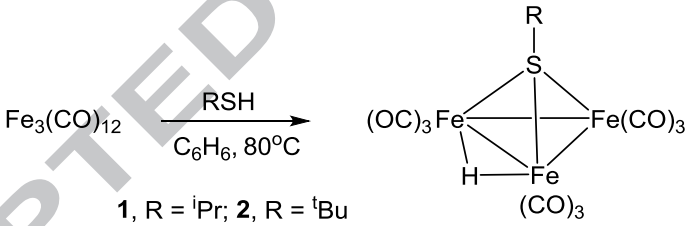

Scheme 1. Synthesis of $[Fe_3(CO)_9(\mu_3\text{-}S^iPr)(\mu\text{-}H)]$ (**1**) and $[Fe_3(CO)_9(\mu_3\text{-}S^tBu)(\mu\text{-}H)]$ (**2**).

Earlier diffraction data for **1** and **2** were collected at room temperature and we thus collected a low-temperature data set for **1,** an ORTEP diagram generated from the new data is shown in Fig. 1. Although we obtained a different polymorph, metric parameters are similar to those reported earlier by Bau *et. al.* [32]. The molecule consists of an isosceles triangle of iron atoms [Fe(1)─Fe(2) 2.6875(5), Fe(1)─Fe(3) 2.6379(5) and Fe(2)─Fe(3) 2.6366(5) Å] coordinated by nine terminal carbonyls, a face-capping isopropyl thiolate ligand, and an edge-bridging hydride. The carbonyls are evenly distributed among three irons and the thiolate ligand asymmetrically caps one face of the metal triangle [Fe(1)─S(1) 2.1411(7), Fe(2)─S(1) 2.1446(6) and Fe(3)─S(1) 2.1203(7) Å]. The hydride, which was located in a difference map and spans the longest Fe─Fe vector, lies on the opposite face of the metallic

plane with respect to the thiolate ligand. The OC─Fe─Fe angles along this particular Fe─Fe edge open up significantly due to the hydride disposition [C(1)─Fe(1)─Fe(2) 105.48(8) and C(4)─Fe(2)─Fe(1) 106.01(9)°] as expected. The ^{1}H NMR spectrum of **1** shows a high-field singlet at –23.76 ppm, consistent with the presence of a bridging hydride, in addition to a septet and a doublet at 4.20 and 1.70 ppm, respectively, with an intensity ratio of 1:6, that are attributed to the methine and methyl protons of the isopropyl thiolate ligand.

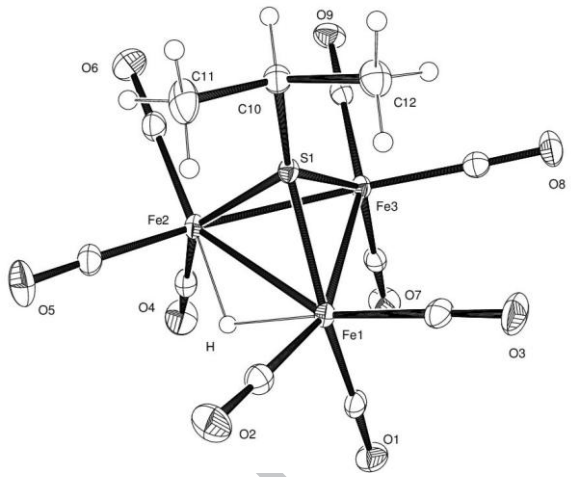

Fig. 1. ORTEP diagram of the molecular structure of $[Fe_3(CO)_9(\mu_3\text{-}S^iPr)(\mu\text{-}H)]$ (**1**). Selected bond distances (Å) and angles (º): Fe(1)─Fe(2) 2.6875(5), Fe(1)─Fe(3) 2.6379(5), Fe(2)─Fe(3) 2.6366(5), Fe(1)─S(1) 2.1411(7), Fe(2)─S(1) 2.1446(6), Fe(3)─S(1) 2.1203(7), Fe(1)─Fe(2)─Fe(3) 59.393(12), Fe(2)─Fe(1)─Fe(3) 59.343(12), Fe(2)─Fe(3)─Fe(1) 61.263(12), Fe(1)─S(1)─Fe(2) 77.67(2), Fe(2)─S(1)─Fe(3) 76.37(2), Fe(3)─S(1)─Fe(1) 76.49(2), S(1)─Fe(1)─Fe(2) 51.224(17), S(1)─Fe(1)─Fe(3) 51.401(18), S(1)─Fe(2)─Fe(1) 51.108(19), C(1)─Fe(1)─Fe(2) 105.48(8), C(4)─Fe(2)─Fe(1) 106.01(9), C(2)─Fe(1)─Fe(2) 102.28(8), C(5)─Fe(2)─Fe(1) 101.85(8).

2.2. Attempted protonation and electrochemistry

Since protonation is a key step in electrocatalytic proton reduction, clusters **1** and **2** were treated with a range of acids [CH_3CO_2H (pK_a ≈ 22.3), CF_3CO_2H (pK_a ≈ 12.7) and $HBF_4{\cdot}Et_2O$ (pK_a ≈ 0.1)] in CH_2Cl_2 [34]. Infrared spectroscopy shows that the clusters do not react with these acids and are stable in acidic solutions. The electrochemical responses of **1** and **2** were next examined by cyclic voltammetry in CH_2Cl_2, and the cyclic voltammograms (CVs) recorded at a scan rate of 0.1 V/s are shown in Fig. 2. Both clusters display a quasi-reversible reduction wave together with a relatively large irreversible oxidative wave. The reversibility of the reductive process of both clusters improves with scan rate, while the

oxidative process remains irreversible at all scan rates (0.025 to 1 V/s) (Figs. S1 and S2). A plot of reductive peak currents against the square root of scan rates indicates that the reductive feature of both clusters originates from a diffusion-controlled process (Fig. S3). The dependence of the current on the scan rate (v) ($i_p/\sqrt{v}$) (Fig. S4) associated with the $0/1^-$ wave for both clusters shows slight deviations from linearity only at very slow scan rates, which indicates that the electrode process tends towards a two-electron transfer on longer time scales.

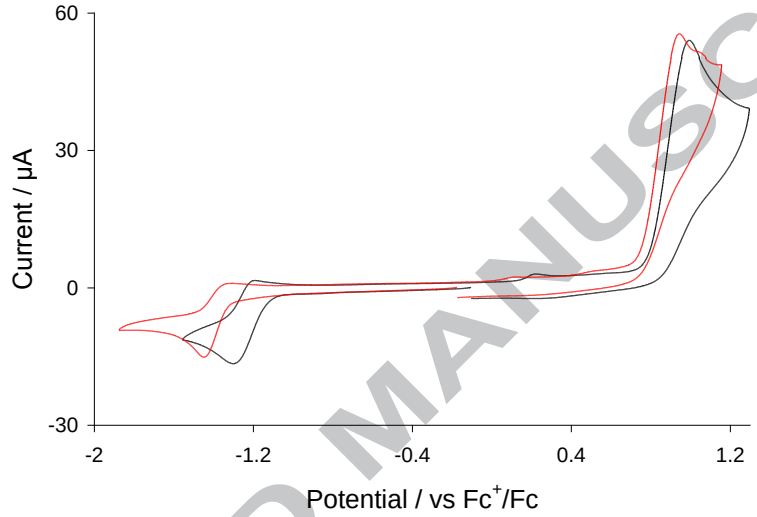

Figure 2. CVs of **1** (black) and **2** (red) in CH_2Cl_2 (1 mM solution, supporting electrolyte $[NBu_4][PF_6]$, scan rate 0.1 Vs^{-1}, glassy carbon electrode, potential vs Fc^+/Fc)

The reduction potential of **2** shows a 160 mV negative shift due to the presence of an additional methyl group on the thiolate ligand ($E_{1/2}$ = –1.24 V for **1** and $E_{1/2}$ = –1.40 V for **2**), but this has little effect on the oxidation potential ($E_{1/2}$ = 0.99 V for **1** and $E_{1/2}$ = 0.93 V for **2**). The peak current of the anodic wave of the reductive process observed on the return scan at scan rate 0.1 V/s is *ca.* 50% compared to that of the cathodic wave on the forward scan (i_{an}/i_{ca} ~ 0.5 for both **1** and **2**), suggesting that the radical anion has limited stability on the CV time scale. In order to gain a better understanding of the redox processes of **1** and **2**, we have calculated the ground-state electronic structure of the related model cluster $[Fe_3(CO)_9(\mu_3\text{-}SMe)(\mu\text{-}H)]$ (**3**). The LUMO of **3** is largely delocalized over the three iron atoms and is antibonding in nature (Fig. 3). The reduction process is not fully reversible based on a current ratio that is less than unity ($i_{an}/i_{ca} < 1$), and the electrochemical data indicate that a secondary chemical process takes place after reduction. Here electron accession is expected to promote a polyhedral expansion of the metallic core. This assumption was subsequently verified when relaxation effects were taken into account in the geometry optimization of the radical anion

derived from **3**. The DFT-optimized structure of $\mathbf{3}^{\bullet-}$ confirms the loss of one of the non-hydride-bridged Fe–Fe bonds (Fig. 4). The orbital composition of the SOMO and LUMO levels in $\mathbf{3}^{\bullet-}$ is in keeping with an expanded cluster polyhedron. We surmise that a similar Fe–Fe bond scission follows reduction of **1** and **2** and accounts for the poor chemical reversibility of the process at slow scan rates (Scheme 2).

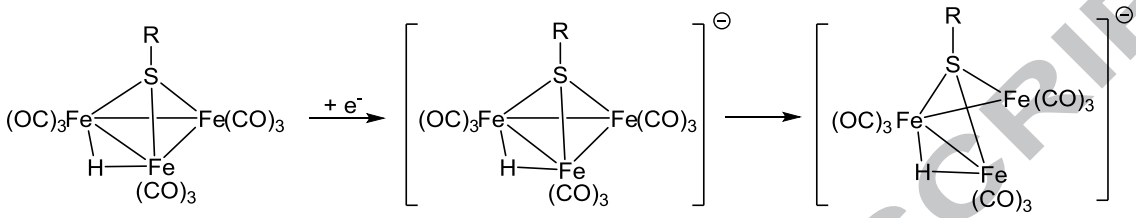

Scheme 2. Reduction of $[Fe_3(CO)_9(\mu_3\text{-SR})(\mu\text{-H})]$ and the proposed chemical process.

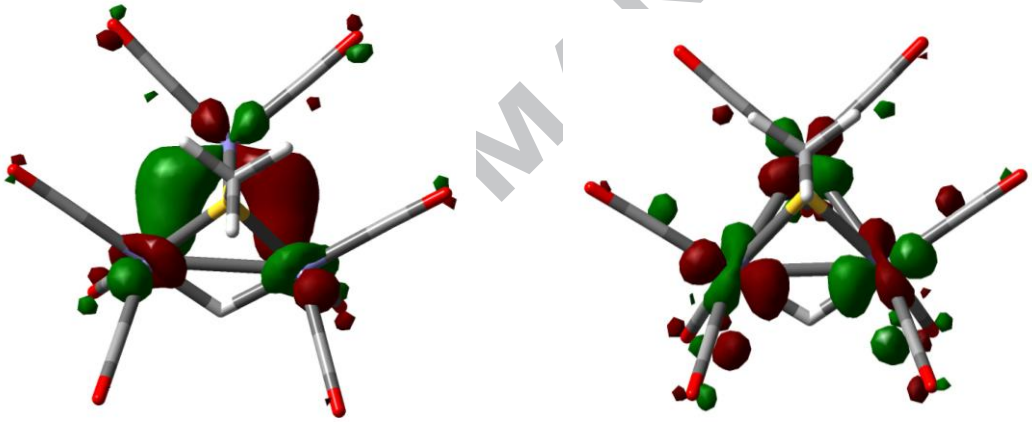

(a) **(b)**

Fig. 3. (a) HOMO and (b) LUMO of $[Fe_3(CO)_9(\mu_3\text{-SMe})(\mu\text{-H})]$ (**3**).

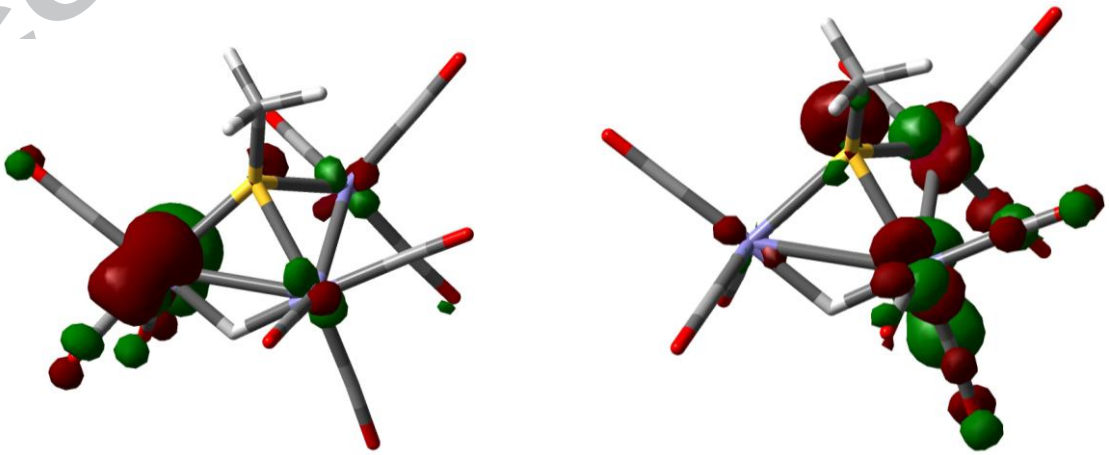

(a) **(b)**

Fig. 4. (a) SOMO and (b) LUMO of $[Fe_3(CO)_9(\mu_3\text{-SMe})(\mu\text{-H})]^-$ ($\mathbf{3}^{\bullet-}$).

2.3. Electrocatalysis

Electrocatalytic testing of **1** and **2** was carried out in CH_2Cl_2 in the presence of CF_3CO_2H and $HBF_4{\cdot}Et_2O$. Both clusters exhibit catalytic waves at their first reduction potential in the presence of acids (Figs. 5 and 6). The catalytic limiting current obtained by using $HBF_4{\cdot}Et_2O$ as the proton source is higher than that obtained with CF_3CO_2H, indicating that the catalytic rate is dependent on acid strength (Fig. S5).

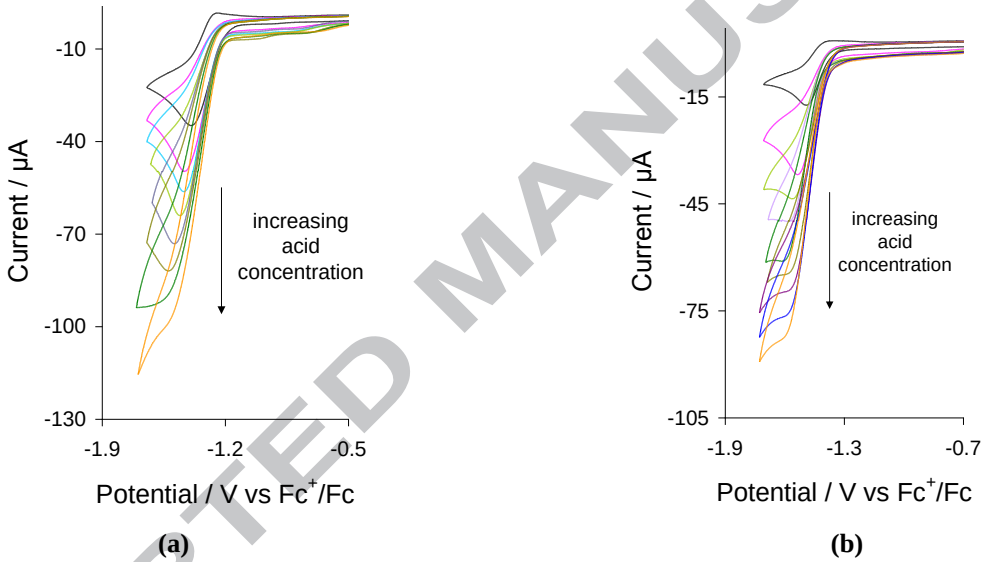

Fig. 5. (a) CVs of **1** in the absence and presence of 1, 2, 3, 5, 6, 8 and 10 molar equivalents of CF_3CO_2H; (b) CVs of **2** in the absence and presence of 1, 2, 3, 4, 5, 6, 8 and 10 molar equivalents of CF_3CO_2H (in CH_2Cl_2, 1 mM solution, supporting electrolyte $[NBu_4][PF_6]$, scan rate 0.1 Vs^{-1}, glassy carbon electrode, potential vs Fc^+/Fc).

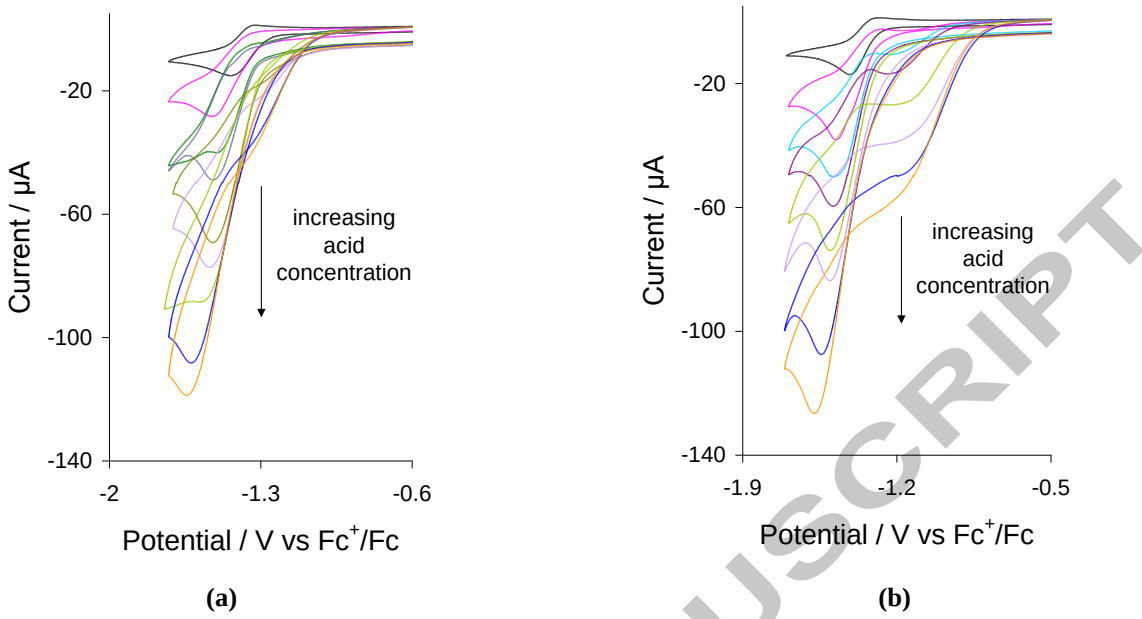

Fig. 6. (a) CVs of **1** in the absence and presence of 1, 2, 3, 4, 6, 8 and 10 molar equivalents of $HBF_4 \cdot Et_2O$; (b) CVs of **2** in the absence and presence of 1, 3, 4, 6, 7, 8, 9 and 10 molar equivalents of $HBF_4 \cdot Et_2O$ (in CH_2Cl_2, 1 mM solution, supporting electrolyte $[NBu_4][PF_6]$, scan rate 0.1 Vs^{-1}, glassy carbon electrode, potential vs Fc^+/Fc).

Since the neutral clusters are not protonated by the acids employed in our studies, we propose an ECEC mechanism for H_2 evolution, as shown in Scheme 3. Catalysis is triggered by the one-electron reduction of the cluster, and this is followed by a protonation to form $[H_2Fe_3(CO)_9(\mu_3\text{-}SR)]$. We suggest that this 49-electron open cluster (since one-electron reduction results in iron-iron bond scission) cannot release hydrogen, so it undergoes further reduction to form the 50-electron species $[H_2Fe_3(CO)_9(\mu_3\text{-}SR)]^-$. The latter species releases hydrogen and forms $[Fe_3(CO)_9(\mu_3\text{-}SR)]^-$, whose protonation then regenerates the starting hydrido cluster. The known anions $[Fe_3(CO)_9(\mu_3\text{-}SR)]^-$, which may be independently prepared from $[Fe_3(CO)_9(\mu_3\text{-}SR)(\mu\text{-}H)]$ by deprotonation using either *n*-C_4H_9Li or C_5H_5Na, form stable salts [33]. Treatment of these anionic clusters with acid regenerates $[Fe_3(CO)_9(\mu_3\text{-}SR)(\mu\text{-}H)]$.

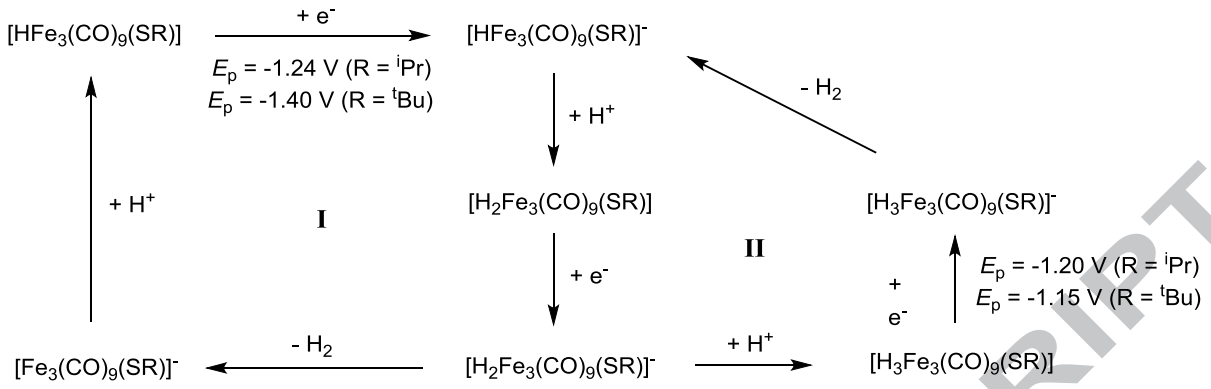

Scheme 3. Proposed mechanism for electrocatalytic proton reduction by $[Fe_3(CO)_9(\mu_3\text{-}SR)(\mu\text{-}H)]$ - only process **I** operates in the presence of weak acids such as CF_3CO_2H, whereas both **I** and **II** operate in the presence of strong acids such as $HBF_4{\cdot}Et_2O$.

CVs of both clusters (especially in the case of **2**) show a build-up of reduction current on the return scan in the presence of $HBF_4{\cdot}Et_2O$ (*ca.* –1.20 V for **1** and *ca.* –1.15 V for **2**). This suggests that a product or intermediate (which can be reduced relatively easily as compared to **1** or **2**, respectively) is also formed during catalysis, possibly *via* a slow chemical reaction, that is sufficiently stable and whose concentration builds up in solution and diffuses back to the electrode for reduction at a more positive potential [35]. We suggest that the release of hydrogen from $[H_2Fe_3(CO)_9(\mu_3\text{-}SR)]^-$ is slow, and thus at higher acid concentrations it undergoes further protonation in the presence of the strong acid $HBF_4{\cdot}Et_2O$ to form $[H_3Fe_3(CO)_9(\mu_3\text{-}SR)]$ which releases hydrogen on the return scan (as shown by process II in Scheme 1).

Figure 7 shows a plot of catalytic current/noncatalytic current (i_{cat}/i_p) ratio against equivalents of acid, and this ratio serves as a measure of catalytic efficiency [36-39]. The i_{cat}/i_p value reaches 3 and 5 for **1** and **2**, respectively, upon the addition of ten equivalents of CF_3CO_2H, whereas the ratio increases to a value of 8 for both clusters upon the addition of a similar amounts of $HBF_4{\cdot}Et_2O$. Since the triiron core of **2** is more basic than that of **1** (*vide supra*), this indicates that the basicity of the cluster core affects the rate of protonation during catalysis when relatively weak acids such as CF_3CO_2H ($pK_a \approx 12.7$) are used. The relevance of the basicity of the cluster core becomes insignificant with strong acids such as $HBF_4{\cdot}Et_2O$ ($pK_a \approx 0.1$). The i_{cat}/i_p ratio is reported within the range 2 to 5 for some of the best diiron biomimics such as $[Fe_2(CO)_5(IMes)(\mu\text{-pdt})]$ (IMes = 1,3-bis(2,4,6-trimethylphenyl)imidazol-2-ylidene; pdt = 1,3-propanedithiolate) [36,37] and $[Fe_2(CO)_3(NO)(\kappa^2\text{-dppv})(\mu\text{-pdt})]^+$ [36,38]

when weak acids are used as a proton source, while the mononuclear nickel complex $[(P^{Ph}{}_2N^{Ph})Ni]^{2+}$ ($P^{Ph}{}_2N^{Ph}$ = 1,3,6-triphenyl-1-aza-3,6-diphosphacycloheptane) [36,39] shows the highest i_{cat}/i_p ratio of 38 reported to date. We wanted to compare the efficiency of these thiolate-capped clusters **1-2** with the sulfido-capped triiron cluster $[Fe_3(CO)_9(\mu_3\text{-}S)_2]$ [19,20], but no such estimation of efficiency had been done for the later. We have carried out a rough comparison of these systems, comparing the catalytic limiting current obtained for $[Fe_3(CO)_9(\mu_3\text{-}S)_2]$ [19] with those of **1-2**. Li *et al.* [19] obtained only *ca.* 30 μA catalytic current at the first catalytic wave after addition of 5 equivalents of $HBF_4{\cdot}Et_2O$, using 4.1 mM of $[Fe_3(CO)_9(\mu_3\text{-}S)_2]$ catalyst (electrode area 1 mm) [19], whereas we obtained *ca.* 60 μA and 70 μA catalytic current after addition of the same amount of $HBF_4{\cdot}Et_2O$ using only a 1 mM catalyst concentration for complexes **1** and **2**, respectively (electrode area 3 mm). The current density calculated for $[Fe_3(CO)_9(\mu_3\text{-}S)_2]$ is ~1900 μAcm^{-2}, while the values are ~425 μAcm^{-2} and ~500 μAcm^{-2} for **1** and **2**, respectively [Here the current density is calculated by dividing the catalytic current observed at half-peak potential in the presence of 5 equivalents acid with the electrode area] [22]. When the difference in concentration of catalysts is taken into account, the current density observed for $[Fe_3(CO)_9(\mu_3\text{-}S)_2]$ and our catalysts (**1** and **2**) becomes quite similar. However, the current at the first catalytic wave saturated after addition of 5 equivalents of acid for $[Fe_3(CO)_9(\mu_3\text{-}S)_2]$, whereas the catalytic current does not show any sign of saturation even after addition of 10 equivalents of $HBF_4{\cdot}Et_2O$ for **1** and **2**. These data suggest that the thiolate-capped triiron clusters **1** and **2** are slightly more efficient catalysts for the reduction of protons than the sulfido-capped cluster $[Fe_3(CO)_9(\mu_3\text{-}S)_2]$ [19,20]. However, the overpotential for electrocatalytic reduction of protons is slightly less for $[Fe_3(CO)_9(\mu_3\text{-}S)_2]$ as compared to **1** and **2** in CH_2Cl_2 in the presence of $HBF_4{\cdot}Et_2O$ as $[Fe_3(CO)_9(\mu_3\text{-}S)_2]$ [19] triggers electrocatalytic proton reduction at –1.03 V, while complexes **1** and **2** operate at –1.24 and –1.40 V, respectively.

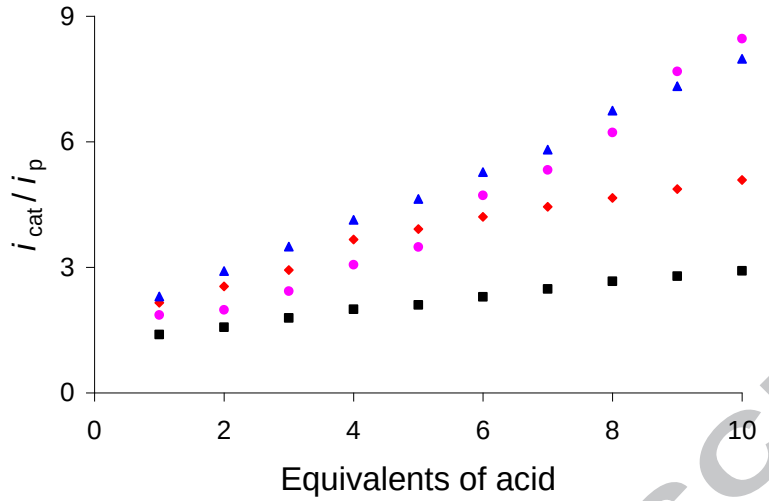

Fig. 7. Dependence of i_{cat}/i_p on acid concentration for **1** [black squares (CF_3CO_2H) and pink circles ($HBF_4{\cdot}Et_2O$)] and **2** [red diamonds (CF_3CO_2H) and blue triangle ($HBF_4{\cdot}Et_2O$)] - (0.5 m*M* solution in acetonitrile, 1-10 m*M* $HBF_4{\cdot}Et_2O$ supporting electrolyte [NBu_4][PF_6], scan rate 0.1 Vs^{-1}, glassy carbon electrode).

3. Summary and conclusions

The thiolate-capped triiron clusters $[Fe_3(CO)_9(\mu_3\text{-}S^iPr)(\mu\text{-}H)]$ (**1**) and $[Fe_3(CO)_9(\mu_3\text{-}S^tBu)(\mu\text{-}H)]$ (**2**), have been tested as electrocatalysts for the reduction of protons to H_2. Cyclic voltammetry shows that their reduction potential is significantly influenced by the substituents on the thiolate-backbone. For both clusters, a relatively slow chemical process takes place after one-electron reduction, the nature of which corresponds to an expansion of the cluster polyhedron through scission of an iron-iron bond, as revealed by electronic structure calculations. Clusters **1** and **2** do not undergo protonation by a wide range of acids and are stable in acidic solution. Both clusters are catalytically active toward proton reduction at their reduction potentials and catalyze H_2 formation from CF_3CO_2H and $HBF_4{\cdot}Et_2O$ through an ECEC mechanism. An additional CECE process is also proposed for H_2 formation from $HBF_4{\cdot}Et_2O$. The catalytic efficiency of both clusters depends on the strength of the acid employed (pH of the solution), and higher catalytic currents were obtained when $HBF_4{\cdot}Et_2O$ was used as the proton source. These thiolate-capped triiron clusters also show slightly enhanced catalytic activity over the sulfido-capped triiron cluster $[Fe_3(CO)_9(\mu_3\text{-}S)_2]$, but these clusters also operate at slightly more negative potential than that of $[Fe_3(CO)_9(\mu_3\text{-}S)_2]$ [19,20].

4. Experimental

4.1. General Methods

All the reactions were carried out under a nitrogen atmosphere using standard Schlenk techniques unless otherwise stated. Reagent-grade solvents were dried using appropriate drying agents and distilled prior to use by standard methods. Infrared spectra were recorded on a Nicolet 6700 FT-IR spectrophotometer. NMR spectra were recorded on a Bruker DPX 400 instrument. **[**$Fe_3(CO)_9(\mu_3\text{-}S^iPr)(\mu\text{-}H)$] (**1**) and [$Fe_3(CO)_9(\mu_3\text{-}S^tBu)(\mu\text{-}H)$] (**2**) were prepared according to a published procedure [29].

*4.2. Synthesis of $Fe_3(CO)_9(\mu_3\text{-}S^iPr)(\mu\text{-}H)$ (**1**)*

A benzene solution (20 mL) of [$Fe_3(CO)_{12}$] (200 mg, 0.398 mmol) and isopropyl thiol (48 μL, 0.512 mmol) was heated to reflux for 1 h. The reaction mixture was then allowed to cool at room temperature and the volatiles removed under vacuum. The residue was chromatographed by TLC on silica gel. Elution with pet ether (40-60) developed five bands on the TLC plate. The first two bands gave two isomers of [$Fe_2(CO)_6(\mu\text{-}S^iPr)_2$] [29] as the major products. The third band gave unconsumed [$Fe_3(CO)_{12}$] while the fourth band afforded [$Fe_3(CO)_9(\mu_3\text{-}S^iPr)(\mu\text{-}H)$] (**1**) (10 mg, 5%) as deep red crystals after recrystallization from hexane/CH_2Cl_2 at 4 ^oC. Spectroscopic data for **1**: IR (νCO, CH_2Cl_2): 2083m, 2046s, 2022s, 2006s, 1954w cm^{-1}. ^1H NMR ($CDCl_3$): δ 4.20 (sep, J 20.4, 13.6, 6.8, 1H), 1.70 (d, J 6.4, 6H), –23.76 (s, 1H).

*4.3. Synthesis of $Fe_3(CO)_9(\mu_3\text{-}S^tBu)(\mu\text{-}H)$ (**2**)*

A benzene solution (20 mL) of [$Fe_3(CO)_{12}$] (200 mg, 0.398 mmol) and *tert*-butyl thiol (128 μL, 1.127 mmol) was heated to reflux for 1 h. A similar work up and chromatographic separation developed five bands on the TLC plate. The first two bands gave two isomers of [$Fe_2(CO)_6(\mu\text{-}S^tBu)_2$] [29] as the major products. The third band gave unconsumed [$Fe_3(CO)_{12}$], while the fourth band afforded [$Fe_3(CO)_9(\mu_3\text{-}S^tBu)(\mu\text{-}H)$] (**2**) (24 mg, 12%) as deep red crystals after recrystallization from hexane/CH_2Cl_2 at 4 ^oC. Spectroscopic data for **2**:

IR (νCO, CH_2Cl_2): 2083m, 2046s, 2023s, 2008s, 1950w cm^{-1}. ^1H NMR ($CDCl_3$): δ 1.75 (s, 9H), –23.71 (s, 1H).

4.4. X-ray crystal structure determination

Single crystals of **1** suitable for single crystal X-ray diffraction analysis were grown by slow diffusion of hexane into CH_2Cl_2 solution at 4 °C. A suitable single crystal of **1** was mounted on a Agilent Super Nova dual diffractometer (Agilent Technologies Inc., Santa Clara, CA) using a Nylon Loop and the diffraction data were collected at 150.0(10) K using Mo-Kα radiation (λ = 0.71073). Unit cell determination, data reduction, and absorption corrections were carried out using CrysAlisPro [40]. The structure was solved with the ShelXS [41] structure solution program using Direct Method and refined with the olex2.refine [42] refinement package using Gauss-Newton minimisation within the Olex2 [43] graphical user interface. Non-hydrogen atoms were refined anisotropically, and hydrogen atoms (except the hydride) were included using a riding model. Crystallographic data for **1**: red block, dimensions 0.55 × 0.43 × 0.25 mm^3, triclinic, space group *P*-1, *a* = 7.7272(4), *b* = 8.5059(4), *c* = 14.0708(5) Å, α = 89.748(3), β = 88.451(4), γ = 73.011(4)°, *V* = 884.14(7) $Å^3$, Z = 2, F(000) 494.6, d_{calc} = 1.8622 g cm^{-3}, μ = 2.587 mm^{-1}. 8397 reflections were collected, 3442 unique [R(int) = 0.0330]. At convergence, R_1 = 0.0301, wR_2 = 0.0631 [$I > 2.0\sigma(I)$] and R_1 = 0.0356, wR_2 = 0.0670 (all data), for 232 parameters.

4.5. Electrochemistry

Electrochemistry was carried out either in deoxygenated CH_2Cl_2 with 0.1 M $TBAPF_6$ as the supporting electrolyte. The working electrode was a 3 mm diameter glassy carbon electrode that was polished with 0.3 μm alumina slurry before each scan. The counter electrode was a Pt wire, and the quasi-reference electrode was a silver wire. All CVs were referenced to the Fc^+/Fc redox couple. An Autolab potentiostat (EcoChemie, Netherlands) was used for all electrochemical measurements. Catalysis studies were conducted by the seriatim addition of CF_3CO_2H or $HBF_4{\cdot}Et_2O$ to the reaction solution.

4.6. Computational methodology

All calculations were performed with the hybrid DFT functional B3LYP, as implemented by the Gaussian 09 program package [44]. This functional utilizes the Becke three-parameter exchange functional (B3) [45], combined with the correlation functional of Lee, Yang and Parr (LYP) [46]. The iron atoms were described by Stuttgart–Dresden effective core potentials (ecp) and an SDD basis set, while the 6-31+G(d′) basis set was employed for the remaining atoms. The reported geometries were fully optimized, and the analytical second derivatives were evaluated and found to possess only positive eigenvalues. The geometry-optimized structures have been drawn with the JIMP2 molecular visualization and manipulation program [47].

Acknowledgements

We thank the Commonwealth Scholarship Commission for the award of a Commonwealth Scholarship to SG and the European Commission for Erasmus Mundus for the award of a post-doctoral fellowships to SBM. MGR acknowledges financial support from the Robert A. Welch Foundation (Grant B-1093). Computational resources through the High Performance Computing Services and CASCaM at UNT are acknowledged. Prof. Michael B. Hall (TAMU) is thanked for providing us a copy of his JIMP2 program, which was used to prepare the geometry optimized structures reported here. SG also thanks The Royal Society for an International Authors Grant, which facilitated the preparation of this manuscript during a visit to Lund University.

Supplementary data

CCDC 1442866 contains supplementary crystallographic data for **1**. This data could be obtained free of charge from the Cambridge Crystallographic Data Centre *via* www.ccdc.cam.ac.uk/ data_request/cif.

References

[1] I.P. Georgakaki, L.M. Thomson, E.J. Lyon, M.B. Hall, M.Y. Darensbourg, Coord. Chem. Rev. 238-239 (2003) 255-266.

[2] D.J. Evans, C.J. Pickett, Chem. Soc. Rev. 32 (2003) 268-275.

[3] T.B. Rauchfuss, Inorg. Chem. 43 (2004) 14-26.

[4] L. Sun, B. Åkermark, S. Ott, Coord. Chem. Rev. 249 (2005) 1653-1663.

[5] X. Liu, S.K. Ibrahim, C. Tard, C.J. Pickett, Coord. Chem. Rev. 249 (2005) 1641-1652.

[6] I. Bhugun, D. Lexa, J.-M. Savéant, J. Am. Chem. Soc. 118 (1996) 3982-3983.

[7] S. Kaur-Ghumaan, L. Schwartz, R. Lomoth, M. Stein, S. Ott, Angew. Chem., Int. Ed., 49 (2010) 8033-8036.

[8] L. Schwartz, P.S. Singh, L. Eriksson, R. Lomoth, S. Ott, *C. R. Chim.* 11 (2008) 875-889.

[9] M. Beyler, S. Ezzaher, M. Karnahl, M.-P. Santoni, R. Lomoth, S. Ott, Chem. Commun. 47 (2011) 11662-11664.

[10] A. Orthaber, M. Karnahl, S. Tschierlei, D. Streich, M. Stein, S. Ott, Dalton Trans. 43 (2014) 4537-4549.

[11] V. Artero, M. Fontecave, C. R. Chimie 11 (2008) 926-931.

[12] S. Roy, S.K.S. Mazinani, T.L. Groy, L. Gan, P. Tarakeshwar, V. Mujica, A.K. Jones, Inorg. Chem. 53 (2014) 8919-8929.

[13] G.P. Connor, K.J. Mayer, C.S. Tribble, W.R. McNamara, Inorg. Chem. 53 (2014) 5408-5410.

[14] S. Gao, J. Fan, S. Sun, F. Song, X. Peng, Q. Duan, D. Jiang, Q. Liang, Dalton Trans. 41 (2012) 12064-12074.

[15] M.J. Rose, H.B. Gray, J. R. Winkler, J. Am. Chem. Soc. 134 (2012) 8310-8313.

[16] M.D. Rail, L.A. Berben, J. Am. Chem. Soc. 133 (2011) 18577-18579.

[17] A.D. Nguyen, M.D. Rail, M. Shanmugam, J.C. Fettinger, L.A. Berben, Inorg. Chem., 52 (2013) 12847-12854.

[18] S. Ghosh, K.B. Holt, S.E. Kabir, M.G. Richmond, G. Hogarth, Dalton Trans. 44 (2015) 5160-5169.

[19] Z. Li, X. Zeng, Z. Niu, X. Liu, Electrochimica Acta 54 (2009) 3638-3644.

[20] C.A. Mebi, K.E. Brigance, R.B. Bowman, J. Braz. Chem. Soc. 23 (2012) 186-189.

[21] W. Gao, J. Sun, M. Li, T. Åkermark, K. Romare, L. Sun, B. Åkermark, Eur. J. Inorg. Chem. (2011) 1100-1105.

[22] M. Kaiser, G. Knör, Eur. J. Inorg. Chem. (2015) 4199-4206.

[23] A. Rahaman, S. Basak-Modi, S. Ghosh, G. Hogarth, E. Nordlander, unpublished.

[24] S. Ghosh, G. Hogarth, K.B. Holt, S.E. Kabir, A. Rahaman, D.G. Unwin, Chem. Commun. 47 (2011) 11222-11224.

[25] A. Rahaman, S. Ghosh, D. Unwin, S. Basak-Modi, K.B. Holt, S.E. Kabir, E. Nordlander, M.G. Richmond, G. Hogarth, Organometallics 33 (2014) 1356-1366.

[26] C. Tard, X. Liu, D. L. C. J. Hughes, Pickett, Chem. Commun. (2005) 133-135.

[27] S. Bruña, I. Cuadrado, E. Delgado, C. J. Gómez-García, D. Hernández, E. Hernández, R. Llusar, A. Martín, N. Menéndez, V. Polo, F. Zamora, Dalton Trans. 43 (2014) 13187-13195.

[28] S. Ghosh, G. Hogarth, J. Organomet. Chem. 851 (2017) 57-67.

[29] J.A. de Beer, R.J. Haines, J. Organomet. Chem. 24 (1970) 757-767.

[30] L.-R. Frank, A. Winter, J. Organomet. Chem. 335 (1987) 249-253.

[31] J. Takács, L. Markó, J. Organomet. Chem. 247 (1983) 223-225.

[32] R. Bau, B. Don, R. Greatrex, R.J. Haines, R.A. Love, R.D. Wilson, Inorg. Chem. 14 (1975) 3021-3025.

[33] A. Winter, L. Zsolnai, G. Huttner, Chem. Ber. 115 (1982) 1286-1304.

[34] All pK_a values reported here were measured in MeCN; K. Izutsu, in 'Acid-Base Dissociation Constants in Dipolar Aprotic Solvents', Blackwell Scientific Publications, Oxford, 1990.

[35] R. Mejia-Rodriguez, D. Chong, J.H. Reibenspies, M.P. Soriaga, M.Y. Darensbourg, J. Am. Chem. Soc. 126 (2004) 12004-12014.

[36] M.J. Rose, H.B. Gray, J. R. Winkler, J. Am. Chem. Soc. 134 (2012) 8310-8313.

[37] J.W. Tye, J. Lee, H.-W. Wang, R. Mejia-Rodriguez, J.H. Reibenspies, M.B. Hall, M. Y. Darensbourg, Inorg. Chem. 44 (2005) 5550-5552.

[38] M.T. Olsen, A.K. Justice, F. Gloaguen, T.B. Rauchfuss, S.R. Wilson, Inorg. Chem. 47 (2008) 11816-11824.

[39] M.L. Helm, M.P. Stewart, R.M. Bullock, M. Rakowski-DuBois, D.L. DuBois, Science 333 (2011) 863-866.

[40] CrysAlisPro; Oxford Diffraction: Yarnton, England, 2015.

[41] G.M. Sheldrick, Acta Crystallogr., Sect. A: Found. Crystallogr. 64 (2008) 112-122.

[42] L.J. Bourhis, O.V. Dolomanov, R.J. Gildea, J.A.K. Howard, H. Puschmann, Acta Cryst. A 71 (2015) 59-75.

[43] O.V. Dolomanov, L.J. Bourhis, R.J. Gildea, J.aK. Howard, H. Puschmann, J. Appl. Crystallogr. 42 (2009) 339-341.

[44] M.J. Frisch *et al.*, Gaussian 09, Revision E.01, Gaussian, Inc., Wallingford, CT, USA, 2009.

[45] A.D. Becke, J. Chem. Phys. 98 (1993) 5648-5652.

[46] C. Lee, W. Yang, R.G. Parr, Phys. Rev. B: Condens. Matter 37 (1988) 785-789.

[47] (a) JIMP2, version 0.091, a free program for the visualization and manipulation of molecules: M.B. Hall, R.F. Fenske, Inorg. Chem. 11 (1972) 768-775;
(b) J. Manson, C.E. Webster, M.B. Hall, Texas A&M University, College Station, TX, 2006, http://www.chem. tamu.edu/jimp2/index.html

Graphic abstract

The redox behaviour and electrocatalytic proton reduction ability of thiolate-capped clusters $[Fe_3(CO)_9(\mu_3\text{-}SR)(\mu\text{-}H)]$ (**1**, R = ^{i}Pr; **2**, R= ^{t}Bu) have been investigated. The thiol substituent has a significant influence on their reduction potentials ($E_{1/2}$ = –1.24 V for **1** and $E_{1/2}$ = –1.40 V for **2** *vs.* Fc^{+}/Fc) but less impact on oxidation potentials ($E_{1/2}$ = 0.99 V for **1** and $E_{1/2}$ = 0.93 V for **2** *vs.* Fc^{+}/Fc). Reduction is quasi-reversible and DFT studies reveal that this is due to scission of an iron-iron bond. While the clusters are not protonated by strong acids they catalyse proton reduction at their first reduction potentials and an ECEC mechanism is proposed.

Highlights

- Electrochemistry of triiron thiolate clusters $[Fe_3(CO)_9(\mu\text{-}H)(\mu_3\text{-}SR)]$
- DFT studies reveal structure of monoanion, $[Fe_3(CO)_9(\mu\text{-}H)(\mu_3\text{-}SR)]^-$
- Monoanions catalysts for proton reduction to give H_2